J Solid State Electrochem (2012) 16:977–983
DOI 10.1007/s10008-011-1460-2

ORIGINAL PAPER

Low-voltage anodized TiO_2 nanostructures studied by alternate current electrochemical microscopy and photoelectrochemical measurements

Marina E. Rincón · Cecilia Cuevas-Arteaga · Mauricio Solís de la Fuente · Arturo Estrada-Vargas · Norberto Casillas · Maximiliano Bárcena-Soto

Received: 21 December 2010 / Revised: 11 March 2011 / Accepted: 6 June 2011 / Published online: 23 June 2011

Abstract This paper presents the characterization of TiO_2 nanostructures obtained by low-voltage anodization using alternate current electrochemical microscopy (AC-SECM) and photoelectrochemical (PEC) measurements. TiO_2 nanostructures were obtained from the exposure of titanium foils to several aqueous acidic solutions of hydrofluoric acid+ phosphoric acid at potentials of 1 to 3 V. Scanning electron microscopy, X ray diffraction, and atomic force microscopy studies evidence the formation of a thin porous amorphous layer (<600 nm) with pore size in the range of 200–1,000 nm. By AC-SECM studies at different bias, we were able to confirm the unambiguous semiconducting properties of as-obtained porous titania films, as well as differences in surface roughness and conductivity in specimens obtained at both potentials. The difference in conductivity persists in air annealed samples, as demonstrated by electrochemical impedance spectroscopy and PEC measurements. Specimens obtained at 3 V show lower photocurrent and dark current than those obtained at 1 V, regardless of their larger conductivity, and we proposed it is due to differences on the oxide layer formed at the pore bottom.

Keywords Porous · Anodization · Titania · Photoelectrochemical

M. E. Rincón · M. Solís de la Fuente
Departamento de Materiales Solares, Centro de Investigación en Energía, Universidad Nacional Autónoma de México,
Av. Xochicalco S/N. Col. Centro,
Temixco, Morelos 62580, Mexico

C. Cuevas-Arteaga
Facultad de Ciencias Químicas e Ingeniería, CIICAP,
Centro de Investigación en Ingeniería y Ciencias Aplicadas,
Universidad Autónoma del Estado de Morelos,
Av. Universidad 1001, Col. Chamilpa,
Cuernavaca, Morelos 62210, Mexico

A. Estrada-Vargas (✉)
Centro Universitario de Ciencias Exactas e Ingenierías,
Departamento de Ingeniería Química,
Universidad de Guadalajara,
Blvd. Marcelino García Barragán 1421,
Guadalajara, Jalisco 44430, Mexico
e-mail: estrad@gmail.com

N. Casillas · M. Bárcena-Soto
Centro Universitario de Ciencias Exactas e Ingenierías,
Departamento de Química,
Universidad de Guadalajara,
Blvd. Marcelino García Barragán 1421,
Guadalajara, Jalisco 44430, Mexico

Introduction

Titania (TiO_2) nanotubular arrays are very interesting materials, whose order, geometry, and dimensions have the potential to outperform titania nanoparticles in multiple applications [1–3]. Electrochemical anodization in acidic solutions is the most recognized method to obtain nanoporous and nanotubular structures. In less than a decade, important knowledge has been gathered around the effect of applied voltage, electrolyte concentration/composition, temperature, and anodization time in the nanoporous and nanotubulars arrays [4–18]. Usually, the fabrication of nanoporous films requires the presence of fluoride (F^-) species, although other electrolytes can be used for this purpose. The most accepted mechanism attributes the formation of tubular structures to competing oxidation and dissolution processes occurring in four stages [15, 17]. Another interesting mechanism proposes the breakdown of the planar oxide/electrolyte interface, indicating that depressions or dents can be formed across the entire surface of the

planar oxide as a consequence of compositional changes in the electrolyte and/or in the oxide that destabilize the planar surface [19]. It has been proposed that the arrays of dents, which lead to nanopores, should form on oxides that chemically dissolve and whose dissolution rate is accelerated by electrolyte species that complex metal cations or catalyze the oxide's chemical dissolution.

Self-organization of nanoporous or nanotubular structures has been obtained in a wide range of potential, from 1 to 60 V, depending on electrolyte and pH of the solution. In electrolytes containing hydrofluoric acid (HF), the dissolution rate is very high, and the anodization has to cease in few minutes, resulting in a limited porous length (around 500 nm), whereas in neutral electrolytes the typical length is in the order of micrometers [5, 9, 10]. Most of the applications of these self-organized structures require thermal treatment to passivate defects and improve on crystallinity. However, annealing leads to the formation of a thick barrier layer between the porous films and underlying Ti substrate, where recombination losses can occur [3]. We have reported the use of as-obtained low-voltage anodized TiO_2 nanostructures as ammonia sensors, founding promising results and clear differences in the sensors prepared at different anodization potential and time [20]. To prepare TiO_2 nanostructures with certain porosity and roughness, we used an aqueous solution of HF and phosphoric acid (H_3PO_4) and followed the procedure reported in [13].

To gather information on the electrochemical properties determining the differences observed in the low-voltage anodized sensors and to assess the surface characteristics and semiconducting properties of the samples, in this contribution, we report the alternating current scanning electrochemical microscopy (AC-SECM) measurements of as-deposited films and compare them with the electrochemical impedance spectroscopy (EIS) and photoelectrochemical (PEC) measurements of annealed films. For AC-SECM experiments, an AC potential is applied to a Pt microelectrode while this is close to the surface. For metal/electrolyte interfaces at high frequencies (i.e., 100 Hz to 100 kHz), most of the impedance comes from the bulk solution, but a measurable fraction is determined by the probe and affected by the local substrate properties (i.e., conductor or insulator) [21]. Given this capability, AC-SECM has been used to investigate precursor sites for metal pitting and localized corrosion on lacquered tinplates [22–24], as well as local impedance mapping on pitted Ti samples immersed in solutions with different ionic strength [25].

Experimental procedure

Sample preparation

High-purity (99.7%) titanium foils with 0.25-mm thickness were cut appropriately to have 1 cm^2 exposed area in contact with the electrolyte. Prior to anodization in a low-voltage potentiostat (ACM Instrument 8AC connected to a personal computer), the samples were mirror polished; degreased in an ultrasonic bath with isopropanol, deionized water, and ethanol; rinsed in deionized water; and dried in a nitrogen stream. To improve the reproducibility of the polished samples prior to anodization, a galvanostatic test was carried out at 3 mA cm^{-2} during 300 s to form a thin oxide layer. Anodization was conducted in a conventional three-electrode configuration, with a platinum grid as counter electrode and Ag/AgCl (1 M KCl) as reference electrode; the distance between anodic and cathodic electrodes was kept in 10 mm. Experiments were carried out at room temperature (25 °C) under aerated, no stirred conditions, in 1 M H_3PO_4/HF solutions, applying a potential ramp from open-circuit potential (OCP) to 1 or 3 V with a sweep rate of 0.5 $V s^{-1}$, and holding it for various times. For the present study, the samples exposed to 3 V were anodized from 10 to 150 min until self-organized porous films were obtained, whereas the samples exposed to 1 V were anodized from 120 to 240 min obtaining self-organized porous structures at the longest time. The experiments were repeated several times, obtaining similar electrochemical behavior in all the experiments. Polarization curves (PC) in different corrosion environments were obtained applying an overpotential of 0 to 3,000 mV at a scan rate of 5 mV s^{-1}.

Surface characterization

Scanning electron microscopy (SEM) images were taken with a LEO 1450VP microscope, while the depth of the porous TiO_2 structures was obtained with a Nanosurf EasyScan atomic force microscope (Nanosurf AG, Switzerland). Film crystallinity was determined by grazing angle X-ray diffraction (XRD) studies (Rigaku Dmax 2200 diffractometer with Cu Kα radiation) using an incident angle of 0.5°.

For surface conductivity, AC-SECM measurements in 1 M KBr solution were obtained by adapting a commercial frequency analyzer interface (Solartron) to a home-made SECM described elsewhere [26]. Pt microelectrodes with diameter of 1.5 and 25 μm were embedded in a glass pipette and employed as probes, using a micropositioner for probe positioning, an A/D card installed in a personal computer for data acquisition, and programs written with the commercial software LabVIEW (version 5.1) from National Instruments. A Pt wire and a standard Calomel electrode were used as counter and reference electrodes, respectively. The sample was left at open-circuit potential, except for experiments where it needed to be polarized and used as counter-electrode.

Photoelectrochemical and electrochemical impedance spectroscopy measurements were carried out in a Gamry (PCI 1129) electrochemical system, in a three-electrode cell

with quartz window, using a graphite bar as counter electrode and Ag/AgCl as reference electrode. For PEC measurements, an Hg lamp (Apex Arc 200W) with 90-mW/cm^2 illumination intensity together with a manual shutter was used to obtain *I–V* curves in 1 M Na_2SO_4 under pulsed illumination/dark conditions. EIS measurements were performed at various DC potentials with a perturbation of 5 mV (rms) amplitude in the frequency range from 30 kHz to 0.01 Hz.

Results and discussion

Previous works have indicated that the pore morphology and key properties of the porous layers depend on a range of electrochemical parameters [9]. As the present work aims at exploring the surface properties of the porous films in more detail, the electrochemical behavior was first characterized using standard electrochemical techniques. Figure 1 shows the polarization curves (PCs) of polished Ti electrodes recorded from 0 to 3 V for three different HF concentrations (0.1, 0.3, and 0.5 wt.%). For comparison, the behavior in 1 M H_3PO_4 (fluoride free) electrolyte is also shown. It can be observed that the corrosion potential became more active and shift to negative values as the concentration of HF increases (from 121 mV for fluoride-free solutions to −955 mV for 0.5 wt.% HF), bringing also an increase in corrosion current density. The shapes of the PCs are similar for solutions without and with 0.1 wt.% HF, showing an active zone followed by a constant limiting current, and finally presenting an active-passive transition zone. In contrast, at higher HF concentrations, the active–passive transition appears at the beginning of the PCs and is followed by a second peak at 250 mV for 0.3 wt.% HF. In the active–passive transition, the corrosion current density decreases from 4.5 to 0.3 mA cm^{-2} for 0.3 wt.% HF, while for 0.5 wt.% HF, it decreases from 17 to 1 mA cm^{-2}. Apparently, HF concentrations <0.1 wt.% render passive

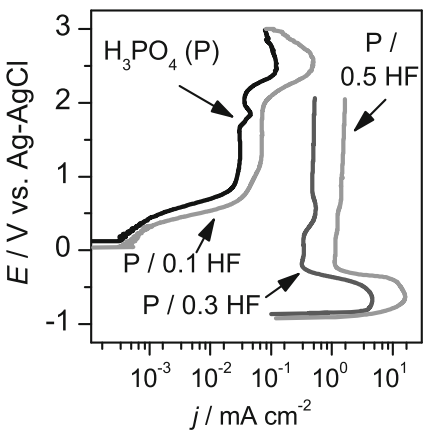

Fig. 1 Polarization curves for titanium exposed to 1 M H_3PO_4 (P) and different concentrations (weight percent) of HF indicated in the figure

systems (i.e., planar oxide films), with corrosion potentials more positive, and corrosion currents one order of magnitude lower, than those obtained at higher HF concentrations. On the contrary, the various oxidation and dissolution currents (i.e., peaks) observed below 2-V polarization in the sample exposed to 3 wt.% HF suggests the formation of self-organized porous structures [13].

Taking into account the previous data, the fabrication of nanostructures was pursued at 1 and 3 V in 1 M H_3PO_4+ 0.3 wt.% HF at ambient temperature. Figure 2 shows such curves, where the typical behavior for the formation of self-organized porous structures is evident [7]. At the beginning and during the first 1,000 s, the current density is small and more or less constant at both potentials, attributing this behavior to the formation of a planar titanium oxide film during the galvanostatic treatment. During the next 2,000 s, the current density suddenly increases up to 0.5–0.6 mA cm^{-2}, due to some surface cracks and narrow slits originated by the field-enhanced dissolution of the oxide layer. Above 3,000 s, it reaches a more or less stable value (0.42–5.0 mA cm^{-2} at 1 V, and 0.52–0.6 mA cm^{-2} at 3 V), but some oscillations are evident in samples anodized at 1 V during longer times (Fig. 2a). The corrosion current at 1 and 3 V was near 0.4–0.5 mA cm^{-2} and 0.5–0.6 mA cm^{-2}, respectively. Sample reproducibility was better for specimens prepared at 3 V, showing self-organized porous structures in a broad interval of anodization times (from 7,200 to 9,000 s), although below 9,000 s, a broad distribution of pore size and patches of non-porous oxide are observed; specimens prepared at 1 V show organized porous structure at anodization times ≥14,400 s.

Differences in porous structure caused by the anodization potential can be appreciated in the SEM images shown in Fig. 3, where the bright/dark contrast correspond to solid/void in the focal plane suggesting pore sizes between 500–1,000 nm (1 V) and 200–500 nm (3 V). Complementary atomic force microscopy (AFM) analyses (Fig. 4) confirm the pore size distribution in the range of 700–900 nm, with heights between 300 and 600 nm for samples prepared at 1 V, while those prepared at 3 V show the pore size distribution in 400–600 nm, with heights between 200 and 500 nm.

In order to correlate the surface conductivity of the samples with their synthesis condition (i.e., anodization potential), the instrument resolution was investigated as a function of microelectrode size and probe-sample distance to optimize the conditions for the AC-SECM analysis. From AC-SECM theory, it is known that the measured impedance at high frequencies is mainly represented by the solution resistance between the tip and the sample, R_S, which is a function of the tip-to-sample distance and the nature of the sample solution. As the tip approaches an insulator, R_S increases because the surface partially blocks some of the pathways for ions to travel between the tip and the counter electrode. Near a

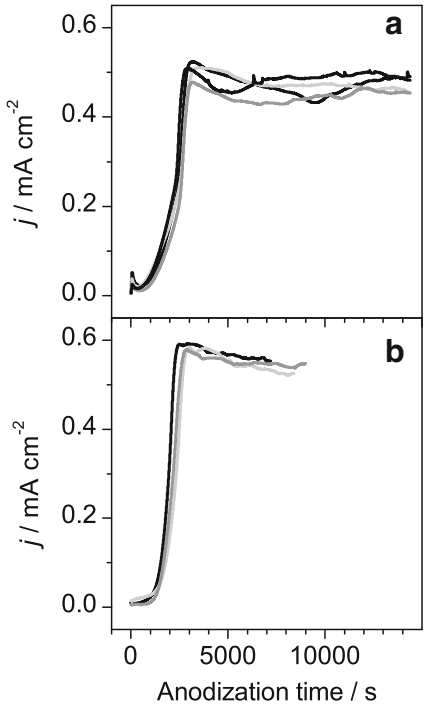

Fig. 2 Anodization curves of Ti exposed to1 M H_3PO_4+0.3 wt.% HF at different potentials: **a** 1 V, **b** 3 V

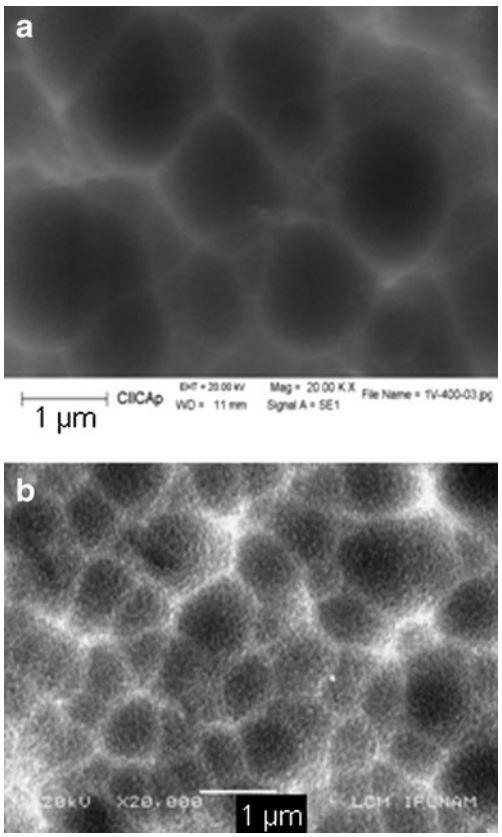

Fig. 3 SEM images of samples anodized at room temperatures in 1 M H_3PO_4+0.3 wt.% HF at 1 V/4 h (**a**) and 3 V/150 min (**b**)

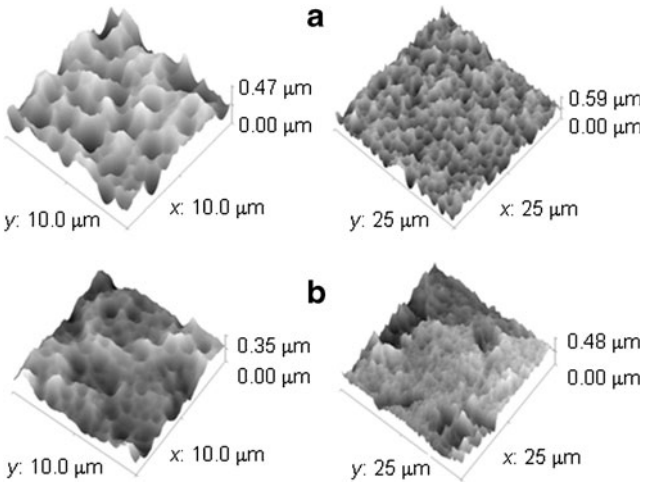

Fig. 4 AFM images of typical topography obtained after an anodization in 1 M H_3PO_4+0.3 wt.% HF at 1 V/4 h (**a**) and 3 V/150 min (**b**)

conducting surface, R_S decreases as the tip approaches the surface because the alternating current can now flow through the conductor; this applies equally whether the conducting sample is used as the counter electrode or is simply left at open circuit [21]. In a two-dimension scan at constant height, the local properties of the sample (i.e., surface roughness and insulating/conducting nature) can be studied as a function of the measured impedance value and topographic or electrochemical maps can be obtained [22–24]. In our studies, an approach curve toward the surface was run prior to mapping in order to fix the probe-sample distance and to assure the passive nature of the porous oxide. Additionally, a contribution from the impedance apparatus to the measured impedance at high frequencies (i.e., >10 kHz) can be expected [27], but the impedance differences due to the film's local conductivity and/or topography are large enough for qualitative analysis [25].

Figure 5 compares the local impedance mapping of porous samples prepared at 1 and 3 V. The maps were obtained with a 1.5-μm probe, applying a 20-mV, 100-kHz AC sinusoidal voltage perturbation, at 0 V vs. open-circuit potential (OCP). No major differences can be appreciated from the images, which show a bumpy surface with high-impedance edges and more conductive bottoms. These differences could be related to differences in sample conductivity or to differences in surface roughness, given that impedance increases as the probe approaches the insulating surface. Samples obtained at 3 V show slightly lower impedances and larger edge–bottom variation (Z=3.3 MΩ/ΔZ=30 kΩ) than those observed in 1-V films (Z=3.5 MΩ/ΔZ=15 kΩ), which is in agreement to their patchy topography (i.e., surface roughness). To further verify that the lower impedance of the sample obtained at 3 V was also indicative of an improved surface conductivity, the impedance of the electrode was measured

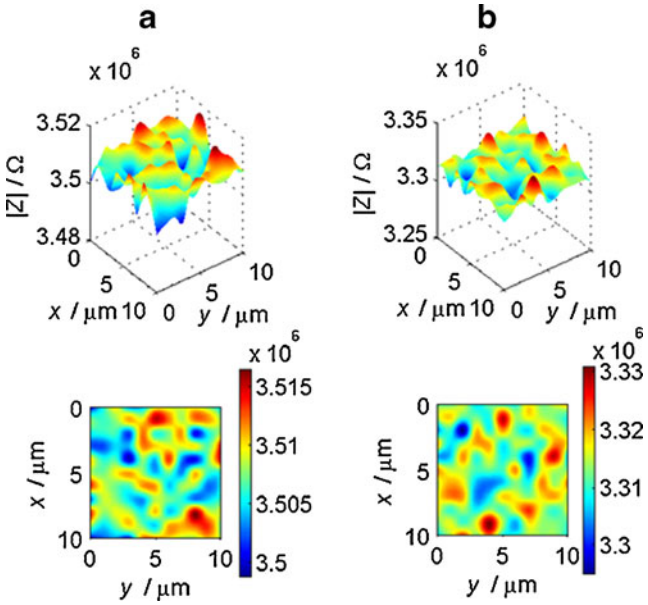

Fig. 5 AC-SECM (1.5 μm probe) of anodized titania porous films obtained at 1 V (**a**) and 3 V (**b**). The approaching curve (not shown) indicates the passive nature of the oxide surface

consecutively under rest potential and at negative DC polarization, as indicated in Fig. 6. Zones of the film with larger impedance appear as lower impedance once the polarization is reversed, i.e., TiO_2 samples behave as insulators when left at OCP and as conductors when polarized, suggesting the transition of the film/electrolyte interface from charge depletion to accumulation. Similar behavior was found in samples anodized at 1 V, confirming

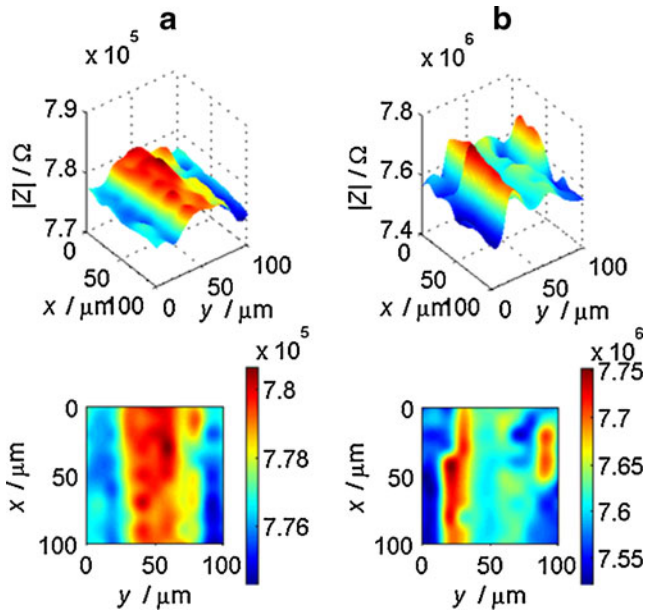

Fig. 6 AC-SECM (25 μm probe) of anodized titania porous films obtained at 3 V. Impedance measurements obtained at rest potential (**a**) and under negative polarization (**b**)

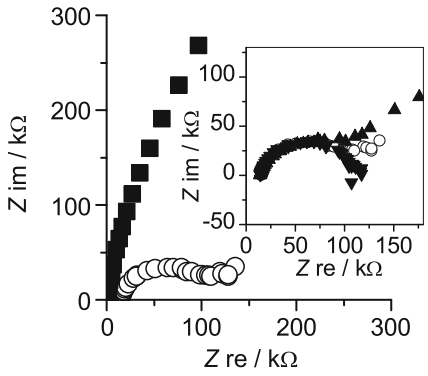

Fig. 7 EIS of air annealed porous films obtained at 1 V (*filled square*) and 3 V (*open circle*). Measurements carried out in 1 M Na_2SO_4 at rest potential. The *inset* shows the effect of DC bias on samples anodized at 3 V: (*filled triangle*) +0.3 V_{DC}, (*open circle*) 0.0 V_{DC}, and (*inverted filled triangle*) −0.3 V_{DC}

the formation of porous titania films with unambiguous semiconducting properties. It is worth to mention the as-deposited nature of the films studied by AC-SECM.

Differences in surface conductivity between the 1- and 3-V anodized films persist after annealing in air at 400 °C for 1 h and testing in a different electrolyte (Na_2SO_4 instead of KBr). Figure 7 shows a Nyquist diagram of EIS experiments scanning the same frequency interval and corresponding to the average response of 1 cm^2 electrodes. The Nyquist plot of the 1-V film is dominated by the complex impedance (capacitive behavior) which is typical of low conductive oxides or blocking electrodes, while the 3-V specimen shows a semicircle intersecting the real axis in the high-frequency region followed by an ion diffusion process at low frequencies. Typically, the semicircle can be fitted by a resistance *Rs* in series with a $R_{CT}C_{DL}$ sub-circuit, where R_S represents the ohmic serial resistance caused mostly by the solution resistance while R_{CT} is the charge-transfer resistance in parallel with the capacitance of the electrical double layer C_{DL}. R_s is slightly higher in 3-V films than in 1-V films, suggesting lower ionic conductivity in their narrower pores. The inset of Fig. 7 shows the effect of potential on the charge transfer resistance and ion diffusion process of films anodized at 3 V. In the polarized samples is interesting to observe that at medium and low frequencies there is a transition from larger to lower impedance under negative polarization, similar to that seen in Fig. 6. This result suggests that the spatial distribution of the semiconducting oxide is been located in the interior of the porous structure (i.e., medium walls or bottom).

EIS measurements agree with the photoelectrochemical results obtained in 1 M Na_2SO_4 (Fig. 8), where the *j–V* curves under dark/illumination conditions show lower current density in samples obtained at 3 V. Dark currents in both specimens are related to charge accumulation (i.e., capacitive current) but in those obtained at 1 V also

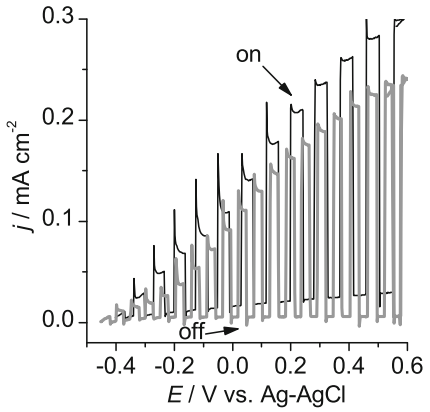

Fig. 8 Photoelectrochemical response of air annealed porous films obtained at 1 V (*black line*) and 3V (*gray line*) in 1 M Na_2SO_4. Illumination intensity, 90 mW/cm^2. Labels *off/on* refer to the condition of the lamp

reflects ohmic drop due to its larger resistivity. Under illumination, the photocurrent density of the more resistive 1-V film is higher than the more conductive 3-V film, ruling out interparticle resistance (i.e., in the neck region) or constrained ion diffusion as the main factors for their large resistivity. Instead, the low electron concentration of the as-deposited and annealed films is again evident. The lower photocurrent of the 3-V film can be due to a higher porosity (less semiconducting solid), different crystallinity, lower area accessible to the hole scavenging electrolyte solution, or to the fact that those surface states increasing the concentration of majority carrier (electrons) can act as trap or increase the recombination rate of photogenerated minority carriers (holes). XRD measurements confirm differences in crystal phases between the 1- and 3-V annealed samples (Fig. 9) The larger intensity of the broad feature at low diffraction angles and the larger relative intensity of the rutile peak at 2θ=63° in 1-V specimens, can be correlated with a major fraction of rutile in these samples. Rutile grows at the interface between the barrier layer and titanium metal [28], and has a lower band gap than anatase. Therefore, the lower fraction of rutile in samples anodized at 3 V can be a factor to explain their lower photocurrent.

The observed differences between the 1- and 3-V films cannot be accounted by differences in surface roughness; chemical differences do exist in both films and persisted after annealing. Apparently, the equilibrium between the chemical and electrochemical processes during film formation causes the abundance of surface defects (i.e., low-coordinated Ti) in samples anodized at 3 V during shorter periods. These defects can be related to the enhanced surface reactivity and surface conductivity of these films, and are not completely passivated after annealing at 400 °C for 1 h. To sort through the origin of the chemical differences, we can take a closer look to the anodization curves in Fig. 2, where a clear difference in the time required to reach the maximum corrosion current is evident. It is a fast process at 3 V, correlated with a larger number of cracks producing a major number of porous, which resulted in smaller diameter. This behavior can be explained by considering that at the beginning of the anodization test, the thin oxide layer formed by the galvanostatic treatment will slowly dissolve locally (i.e., at the cracks), and the field strength inside the oxide thus increases. Under equal chemical dissolution rates, the local critical field strength for electrical breakdown and current flow will be reached faster in the specimen anodized at 3 V. Once the initial morphology sets up, dissolution rates can no longer be assumed equal, due to differences in the reactant/product concentration, which magnifies as the difference in pore diameter increases [19]. The different acidification of the oxide/electrolyte interface (i.e., H^+/OH^- will be determined by the rates of chemical oxide dissolution/electrochemical oxide formation) will lead to compositional changes in the oxide, favoring the formation of surface defects in the 3-V specimens. The larger number of cracks in samples anodized at 3 V could also be related to the larger electric field strength in these samples.

Conclusions

Experimentation was carried out with the aim to study in more detail the surface properties of as-prepared porous TiO_2 anodized at low potential (<3 V) in a H_3PO_4/HF aqueous solution. By alternating current scanning electrochemical microscopy at different bias, it was possible to confirm the formation of porous titania films with clear semiconducting properties, and differences in surface roughness and surface conductivity in specimens obtained at 1 and 3 V. Differences in surface conductivity originate from differences in surface defects, which are not fully passivated after annealing. Electrochemical impedance and

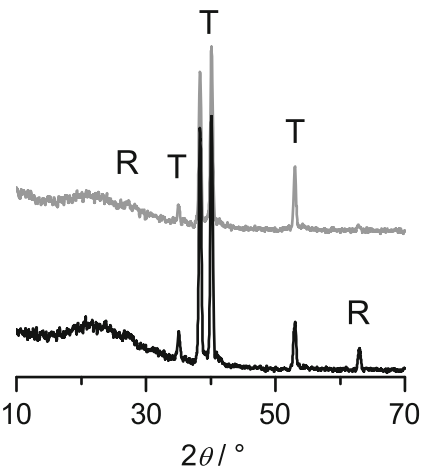

Fig. 9 XRD spectra of air annealed porous films obtained at 1 V (*black line*) and 3 V (*gray line*) in 1 M Na_2SO_4. *T* titanium, *R* rutile

photoelectrochemical measurements of samples obtained at the higher potential suggest a more conductive and reactive interface at the pore bottom which also acts as a recombination interface for photogenerated holes, explaining their lower current under dark and illumination conditions.

Acknowledgments Financial supports from Dirección General de Asuntos del Personal Académico de la Universidad Nacional Autónoma de México (DGAPA-UNAM, IN104309) and Consejo Nacional de Ciencia y Tecnología-México (CONACyT, 49100) are gratefully acknowledged, as well as the fellowship (MSF) provided by CONACyT-México. We thank A. Adaya and M. Sánchez for sample preparation and analyses.

References

1. Lee WJ, Alhosan M, Yohe SL, Macy NL, Smyrl WH (2008) J Electrochem Soc 155:B915–B920
2. Park JH, Kim S, Bard AJ (2006) Nano Lett 6:24–28
3. Shankar K, Basham JI, Allam NK, Varghese OK, Mor GK, Feng X, Paulose M, Seabold JA, Choi KS, Grimes CA (2009) J Phys Chem C 113:6327–6359
4. Zwilling V, Darque-ceeretti E, Boutry-Forveille A, David D, Perrin MY, Aucouturier M (1999) Surf Interface Anal 27:629–637
5. Gong D, Grimes CA, Varghese OK, Hu WC, Singh RS, Chen Z, Dickey EC (2001) J Mater Res 16:3331–3334
6. Mor GK, Varghese OK, Grimes CA (2003) J Mater Res 18:2588–2593
7. Varghese OK, Gong D, Paulose M, Ong KG, Dickey EC, Gimes CA (2003) Adv Mater 15:624–627
8. Macak JM, Sirotna K, Schmuki P (2005) Electrochim Acta 50:3679–3684
9. Macak JM, Tsuchiya H, Schmuki P (2005) Angew Chem Int Ed 44:2100–2102
10. Taveira LV, Macak JM, Tsuchiya H, Dick LFP, Schmuki P (2005) J Electrochem Soc 152:B405–B410
11. Macak JM, Tsuchiya H, Berger S, Bauer S, Fujimoto S, Schmuki P (2006) Chem Phys Lett 428:421–425
12. Beranek R, Hildebrand H, Schmuki P (2006) Electrochem Solid-State Lett 6:B12–B14
13. Bauer S, Cléber S, Schmuki P (2006) Electrochem Commun 8:1321–1325
14. Macak M, Gong BG, Hueppe M, Schmuki P (2007) Adv Mater 19:3207–3031
15. Yasuda K, Macak JM, Berger S, Ghicov A, Schmuki P (2007) J Electrochem Soc 154:C472–C478
16. Seyeux A, Berger S, LeClere D, Valota A, Skeldon P, Thompson GE, Kunze J, Schmuki P (2009) J Electrochem Soc 156:K17–K22
17. Thébault F, Vuillemin B, Oltra R, Kunze J, Seyeux A, Schmuki P (2009) Electrochem Solid-State Lett 12:C5–C9
18. Oyarzún DP, Córdova R, Linarez-Pérez OE, Muñoz E, Henríquez R, López-Teijelo M, Gómez H (2010) Morphological, electrochemical and photoelectrochemical characterization of nanotubular TiO2 synthetized electrochemically from different electrolytes. J Solid State Electrochem. doi:10.1007/s10008-010-1236-0
19. Nguyen QAS, Bhargava YV, Devine TM (2009) J Electrochem Soc 156:E55–E61
20. Sánchez M, Cuevas C, Rincón ME (2010) ECS Trans 28:9–18
21. Horrocks BR, Schmidtke D, Heller A, Bard AJ (1995) Anal Chem 65:3605–3614
22. Ballesteros-Katemann B, Schulte A, Calvo EJ, Koudelka-Hep M, Schuhmann W (2002) Electrochem Commun 4:134–138
23. Ballesteros-Katemann B, Inchauspe CG, Castro PA, Schulte A, Calvo EJ, Schuhmann W (2003) Electrochim Acta 48:1115–1121
24. Eckhard K, Kranz C, Shin H, Mizaikoff B, Schuhmann W (2007) Anal Chem 79:5435–5438
25. Estrada-Vargas A, Ávalos J, Bárcena-Soto M, González I, Antaño R, Casillas N (2006) 210th meeting of the the Electrochemical Society, Abstract 0057
26. Hernández-Ramírez F (2001) Diseño, construcción y caracterización de un microscopio electroquímico y fotoelectroquímico de barrido. Master thesis, Universidad de Guadalajara, Guadalajara
27. Diakowski PM, Baranski AS (2006) Electrochim Acta 52:854–862
28. Mor GK, Varghese OK, Paulose M, Shankar K, Grimes CA (2006) Sol Energ Mat Sol C 90:2011–2075